Optical waveplates based on birefringence of anisotropic two-dimensional layered materials

He Yang, [†] Henri Jussila, [†] Anton Autere, [†] Hannu-Pekka Komsa, [‡] Guojun Ye, [∥, ⊥]

Xianhui Chen, [∥, ⊥, §] Tawfique Hasan,[¶] and Zhipei Sun *,[†]

[†]Department of Electronics and Nanoengineering, Aalto University, Espoo, FI-00076, Finland

[‡]Department of Applied Physics, Aalto University, Espoo, FI-00076, Finland

[∥]Hefei National Laboratory for Physical Science at Microscale and Department of Physics, University of Science and Technology of China, Hefei 230026, China

[⊥]Key Laboratory of Strongly-Coupled Quantum Matter Physics, University of Science and Technology of China, Chinese Academy of Sciences, Hefei 230026, China

[§]Collaborative Innovation Center of Advanced Microstructures, Nanjing 210093, China

[¶]Cambridge Graphene Centre, Department of Engineering, University of Cambridge, Cambridge CB3 0FA, UK

ABSTRACT: Birefringence is an inherent optical property of anisotropic materials introduced by the anisotropic confinement in their crystal structures. It enables manipulation of light propagation properties (e.g., phase velocity, reflection, and refraction) for various photonic and optoelectronic applications, including waveplates and liquid crystal displays. Two-dimensional (2D) layered materials with high anisotropy are currently gaining an increasing interest for polarization-integrated nano-device applications, which advances the research on birefringent materials. In this article, we investigate the optical birefringence of three anisotropic 2D layered materials (black phosphorus (BP), rhenium disulfide (ReS_2), and rhenium diselenide ($ReSe_2$)). We demonstrate that the birefringence in BP (~0.245) is ~ 6 times larger than that of ReS_2 (~0.037) and $ReSe_2$ (~0.047) at 520 nm and is comparable to the current state of the art bulk materials (e.g., $CaCO_3$). We use these 2D materials to fabricate atomically-thin optical waveplates and investigate their performance. In particular, for BP, we observe a polarization-plane rotation of ~0.05° per atomic layer at 520 nm. Our results show that the relatively large birefringence of anisotropic 2D layered materials can enable accurate manipulation of light polarization with atomically controlled device thickness for various applications where integrated, nanoscale polarization-controllers are required.

Recently, anisotropic two-dimensional (2D) layered materials are gaining an increasing amount of interest to fabricate anisotropic nano-devices for various applications. For example, black phosphorus (BP),[1-6] the most widely studied anisotropic 2D material, has a puckered hexagonal crystal structure with two non-equivalent in-plane crystal directions (armchair (AC) and zigzag (ZZ)[7]; Figure 1a), different from graphene[8-10] and typical transitional metal dichalcogenides (e.g., MoS_2 and WSe_2).[11-20] As with the crystal structure, the physical properties of BP (e.g., electrical,[2] mechanical,[4] thermal,[21]) are also anisotropic. ReS_2 and $ReSe_2$ are two examples of other anisotropic 2D material. They also demonstrate anisotropic responses arising from their in-plane anisotropic structure.[22-28] These 2D materials also have been demonstrated to have a strong anisotropic optical conductivity. For example, BP exhibits anisotropic linear (e.g., absorption,[29] photoluminescence,[7, 30, 31] optical contrast,[29] and optical phase[32]) and nonlinear optical responses (e.g., Raman scattering,[33-38] saturable absorption,[39] and harmonic generation[40]). These anisotropic responses open up

possibilities for integrated, polarization-dependent, novel optical devices, including polarization-sensitive broadband photodetectors,[31, 41] and linearly-polarized ultrafast lasers.[39, 42] However, such devices have not yet been realised.

In this article, we demonstrate atomically-thin optical waveplates based on the optical birefringence of three typical anisotropic 2D materials (BP, ReS_2 and $ReSe_2$) in the visible spectral range. Among the three materials investigated, the waveplate performance (i.e., phase retardance, polarization-plane rotation angle) from BP is superior to that of ReS_2 and $ReSe_2$. Our experiments show that the birefringence in BP (~0.245) is ~ 6 times larger than that in ReS_2 (~0.037) and $ReSe_2$ (~0.047) at 520 nm wavelength. We also demonstrate a polarization-plane rotation of ~0.05°, 0.02° and 0.011° per atomic layer (AL) at the same wavelength when linearly polarized light propagates through BP, ReS_2 and $ReSe_2$ flakes, respectively. Our results show that the performance on polarization control from BP is comparable to that of the current state of the art bulk materials (e.g. $CaCO_3$) and could be very attractive for integrated polarization-controllers (e.g. waveplates, phase

compensator), where the light polarization state requires precise adjustments at the nanometer scale.

RESULTS AND DISCUSSION

Crystal orientation determination. All the samples studied in this work are fabricated using the micromechanical exfoliation method[43, 44] and then transferred onto transparent quartz substrates. The thickness of the flakes is measured by Atomic Force Microscopy, with detailed measured results shown in Supporting Information (SI).

Like other anisotropic 2D materials, the highly asymmetric crystal structure in BP enables its strong in-plane anisotropic optical response. For example, the Raman spectra of BP show strong polarization dependence, similar to one-dimensional nanomaterials (e.g. carbon nanotubes[45-47]). This can be used to determine the crystal orientation of BP and other anisotropic crystals.[33-35] Typical Raman spectrum (Figure S1 in SI) of a BP flake shows three Raman modes at 363 cm^{-1}, 440 cm^{-1}, and 468 cm^{-1}, corresponding to the A_g^1, B_{2g}, and A_g^2 vibration modes, respectively.[48] The atomic motion associated with the A_g^2 mode occurs primarily along the AC direction. Thus the associated Raman scattering intensity is the strongest when the excitation laser polarization is aligned with the AC direction.[33] The intensity of the A_g^2 mode can therefore be used to determine the crystal orientations of the BP flakes. In our polarization-resolved Raman experiment, the excitation light is linearly polarized

and the polarization analyser is kept parallel to the polarization direction of the excitation light. The crystal orientations are then determined by rotating the BP flakes and measuring the angular dependence of Raman scattering intensity of the in-plane A_g^2 mode. As measured, the angular dependence of the A_g^2 mode intensity of the selected BP flake is shown in Figure 1b. This demonstrates that the AC direction of this BP sample is parallel with the direction of the excitation laser polarization when the BP flake is rotated by 90° (or 270°). Using a similar strategy, we also use Raman to determine the crystal orientation of ReS$_2$ and ReSe$_2$. Details on the polarization-depended Raman measurements of the three crystals are presented in SI.

Polarization-resolved optical microscopy (PROM) is an alternative tool to determine the crystal orientation of anisotropic crystals.[34] Figure 1c shows the transmitted PROM images of a BP flake as a function of the flake rotation angle under crossed-polarized light illumination. In this case, the polarizer and the analyser in the PROM are set perpendicular to each other. The flake image is recorded by a CCD camera with 15° rotation steps. The flake brightness appears the highest when the crystal axis direction is 45° (and 135°) with respect to the incident polarization direction, while no contrast from the BP flake is observed when one of the crystal axes is parallel to the polarizer direction (i.e., 0° and 90°). This phenomenon originates from the birefringence of BP crystals. It could be explained as follows: when the polarized direction of the incident light is along the AC (or ZZ) direction, the output polarization is unchanged, still perpendicular to the polarization direction of
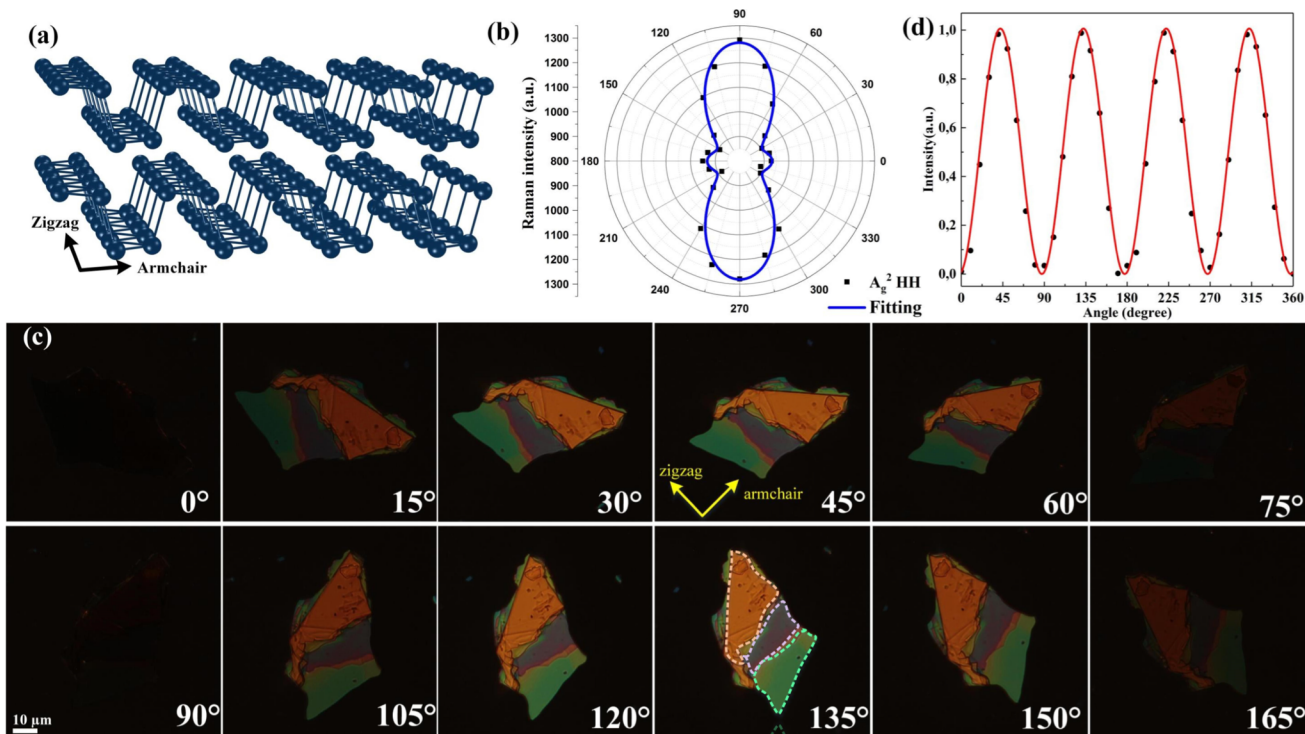
Figure 1 Anisotropic optical properties of BP. (a) Schematic structure of BP; (b) A_g^2 mode intensity with different input polarization angles. Both polarization directions of the excitation laser and the analyser are horizontal in the polarized Raman measurement. (c) Transmitted polarization-resolved optical images under crossed-polarized light illumination in the PROM (i.e., the polarization direction of the incident light and the polarization analyser is perpendicular to each other) with the BP flake rotation angle from 0° to 180°. The step of rotation angle is 15°. The thickness of the flake area marked with the green, purple and yellow boxes is ~45, 35 and 220 nm, respectively. (d) The transmitted light intensity as a function of BP rotation angle (corresponding to Figure 1c) under crossed polarization illumination. The red line depicts the fitting result.
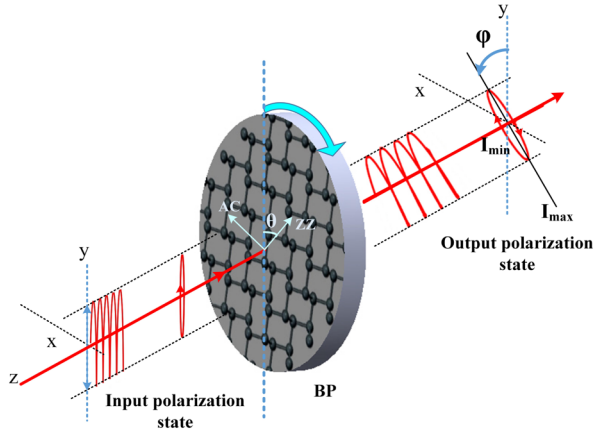
Figure 2 Schematic diagram of the birefringence measurement. A nearly linearly polarized input light has an incident angle θ (with measurement error of ±1°) with respect to the BP's ZZ axis. After propagating through the BP flake, the incident polarization state typically changes to be elliptical, and the output polarization-plane rotates by an angle of φ (with measurement error of ±1°). I_{max} and I_{min} correspond to the maximum and minimum transmitted intensity that is experimentally measured by rotating a polarization analyzer.

the analyser. Therefore, the image is dark. However, when the incident polarization direction has an angle of 45° (or 135°) to the BP crystal axis, the light intensity experiences the maximum phase retardance. This changes the incident polarization state into the elliptical. Thus the light intensity along the polarization direction of the analyser increases to the maximum, corresponding to the brightest flake image. Similarly, for the case of reflection mode, the brightness of the images also changes with the rotation angle of the flake (see Figure S3 in SI). Note that the flake colors at different flake thicknesses are different under the same measurement conditions. For example, Figure 1c mainly presents three colors - green, yellow and purple (marked with different dotted boxes), originating from the interference effect on the flake with different thicknesses.[49] Using these colors, it is possible to estimate the sample thickness.[50, 51]

For ReS₂ and ReSe₂, similar measurements on their PROM images (Figure S5 for ReS₂, Figure S7 for ReSe₂) are also carried out (details in SI). The optical contrast from ReS₂ and ReSe₂ is weaker than that from BP when the PROM images are compared. This suggests that the birefringence of ReS₂ and ReSe₂ is smaller than that of BP.

To quantitatively describe the birefringence-induced transmitted light intensity change, we use a custom-build PROM to measure the maximum transmitted light intensity as a function of the flake rotation angle (see Figure 1d). The diameter of the beam spot on the flakes is ~10 μm, much smaller than the 2D flakes we use in the experiments. As shown in Figure 1d, the transmitted intensity changes periodically with the flake rotation angle with a period of 90°. Further, the transmitted intensity is the lowest when the BP flake is rotated by 0 and 90°. When the flake is rotated by 45° with respect to the incident light polarization, the transmitted light intensity through the BP flake is the highest, as illustrated in Figure 1c. These results suggest strong bire-

fringence of the BP flakes. This is consistent with the discussion above and can be used for the determination of the crystal axis orientation. The red line in Figure 1d is the fitting of the transmitted light intensity following the equation $T = \alpha \sin^2(2\theta)$, where the coefficient α is the total transmittance along the AC and ZZ axes. The fit gives α = ~0.97 for our ~45 nm BP flake, consistent with previous absorption measurement results.[32] We also measure other anisotropic (i.e. ReS₂ and ReSe₂) and isotropic (e.g., MoS₂) 2D materials. Similar intensity modulation property (as shown in Figure 1d) is also observed with ReS₂ and ReSe₂, but not with MoS₂. This highlights the intrinsic optical birefringence of the anisotropic 2D materials we study here. Nevertheless, we note that the crystal orientation of BP, ReS₂ and ReSe₂ can be determined by the PROM approach. The results from the PROM method also match well with the Raman measurements (Table S1 in SI). However, compared with the Raman method, the PROM approach is more cost-effective as it doesn't need a specific laser source and a spectrum analyser which are typically needed in Raman spectroscopy.

Birefringence of anisotropic 2D materials. To quantitatively characterize the birefringence of the anisotropic 2D materials we study, we measure the phase shift (i.e., the phase retardance) between two polarization components projected along two different crystallographic orientations when a linearly-polarized beam is passed through the materials; see the schematic diagram in Figure 2. The polarization of the transmitted light is examined through a polarization analyser. By rotating the analyser (Figure S8 in SI), the maximum (I_{max}) and minimum (I_{min}) transmitted light power is recorded by a power detector to analyze the polarization state of the output light. In this case, I_{max} stands for the intensity along the long-axis (i.e., ZZ direction), while I_{min} for the short-axis (i.e., AC direction). Therefore, the polarization ellipticity (e) of the light after passing through the flake can be calculated by the intensity ratio between the long and short axes (i.e., $e = I_{max}/I_{min}$) for birefringence characterization.

Figure 3a presents the ellipticity change as a function of the flake rotation angle (θ) after the light passes through a ~45 nm thick BP flake at three different wavelengths. It can be seen that the ellipticity is the highest when the flake rotation angle (θ) is either 0° or 90°. This is expected as no phase retardance occurs. In this case, when the incident light is linearly polarized along the ZZ (or AC) direction, no light is projected along the AC (or ZZ) direction. Thus I_{min} is nearly zero when rotating the analyser. However, the ellipticity values at $\theta = 0°$ and 90° are different. For instance, the ellipticity is ~1522 at $\theta = 0°$, and ~850 at $\theta = 90°$ at 520 nm wavelength (Figure 3a). This is because of the dichroic absorption (the absorption difference along two crystal axes) of BP. Comparing the ellipticity values at these two angles (i.e., $\theta = 0°$ and 90°), the magnitude of the dichroic absorption can be extracted. From this, we find that the transmittance ratios between AC and ZZ axes are ~88.7%, ~93.0%, and ~95.9% for 520 nm, 642 nm, and 730 nm, respectively. This agrees well with the previous measurement.[29] On the other hand, when θ is in between 0° and 90°, the ellipticity value decreases rapidly due to the birefringence. Note that we also measure the ellipticity change of two isotropic MoS₂
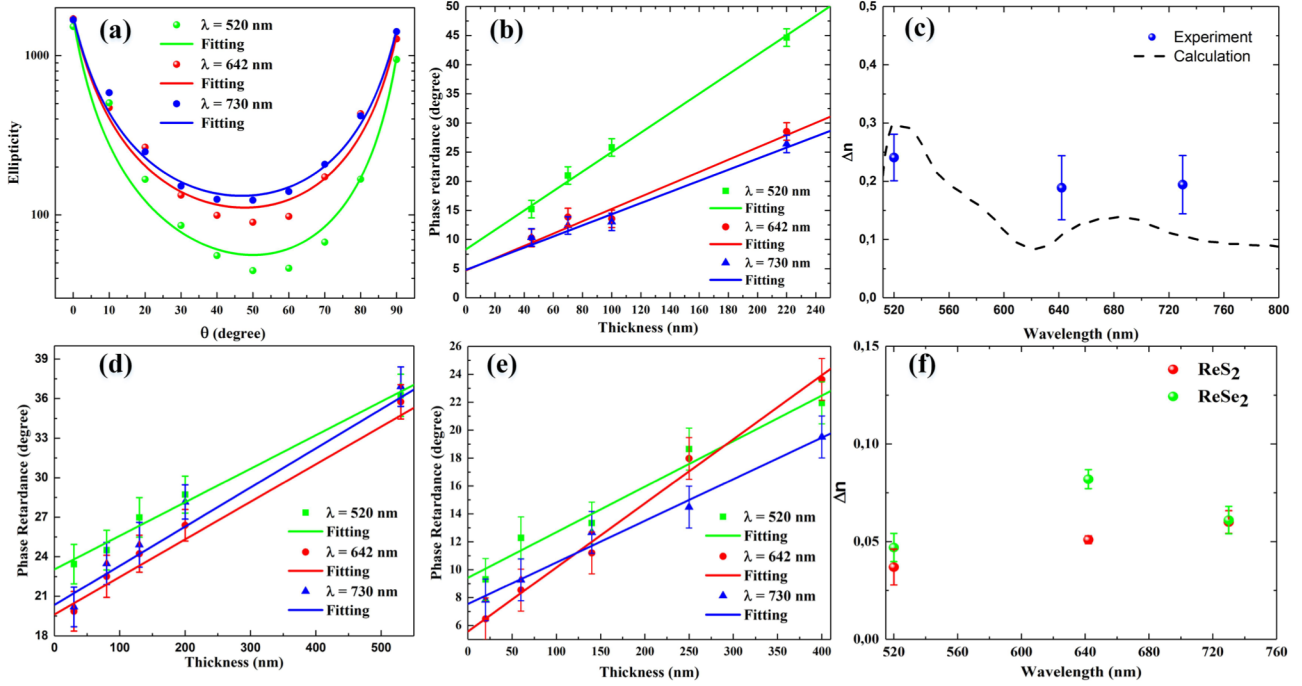
Figure 3 Birefringence of anisotropic 2D materials. (a) The measured light ellipticity (dots) and its fitting (lines, following eq 1) as a function of rotation angle after the light propagates through a ~45 nm BP flake at different wavelengths. (b) Phase retardance as a function of BP flake thickness. (c) Birefringence (Δn) of BP at different wavelengths (Experimental results: Dots; Theoretical results: lines). The phase retardance and their fittings as a function of ReS$_2$ (d) and ReSe$_2$ (e) flake thickness at three wavelengths in the visible range. (f) Experimental results of the birefringence of ReS$_2$ and ReSe$_2$.

flakes (Figure S9 in SI), showing that the ellipticity value remains constant with the rotation of the flake. This confirms that only anisotropic 2D materials have birefringence.

To accurately obtain the value of the birefringence, we use BP as an example to fit the ellipticity change (Figure 3a), using the following equation:

$$\sqrt{e} = \frac{1+s\sqrt{1-4sin^2\delta\frac{A_{ZZ}^2 A_{AC}^2}{(A_{ZZ}^2+A_{AC}^2)^2}}}{1-s\sqrt{1-4sin^2\delta\frac{A_{ZZ}^2 A_{AC}^2}{(A_{ZZ}^2+A_{AC}^2)^2}}} \quad (1)$$

where s = 1 for $A_{ZZ}^2-A_{AC}^2 \geq 0$ and s = -1 for $A_{ZZ}^2-A_{AC}^2 < 0$. A_{AC} and A_{ZZ} are the amplitude of the transmitted light projected along the AC and ZZ directions, respectively, with the consideration of θ and the transmission coefficient along the AC and ZZ crystal axes separately. δ is the phase retardance between the AC and ZZ axes after light propagates through BP flakes. In our model, the incident light is normal to the flake surface, and the dichroic absorption is also considered in the fit. Detailed discussion on the model and eq 1 is presented in SI.

The ellipticity fitting of the ~45 nm thick BP flake is presented in Figure 3a by solid lines, matching well with the measured ellipticity values. The fitted phase retardance δ with eq 1 at three wavelengths is plotted in Figure 3b, where the error bars are from the deviation of the fitting. In addition, BP flakes with other different thicknesses (i.e., 70 nm, 100 nm, and 220 nm) are also characterized and shown for comparison (see Figure S10 in SI). As seen in Figure 3b, the phase retardance increases linearly with the flake thickness, following the equation:

$$\delta(d) = \frac{2\pi \times \Delta n}{\lambda} d + \delta_0 \quad (2)$$

Table 1. Comparison of Δn from different materials

	520 nm	642 nm	730 nm	Reference
BP	0.245±0.04	0.196±0.055	0.202±0.05	This work
ReS$_2$	0.037±0.009	0.051±0.002	0.060±0.006	This work
ReSe$_2$	0.047±0.007	0.082±0.004	0.061±0.007	This work
BP	0.23	0.12		Ref. 29
CaCO$_3$		0.172 (590 nm)		Ref. 56
LiNbO$_3$		0.085 (590 nm)		Ref. 56
SiO$_2$		0.009 (590 nm)		Ref. 56

where $\delta(d)$ is the fitted phase retardance, δ_0 is the phase retardance of the incident polarized light before the BP flake, Δn is the birefringence, characterized by the refractive index difference between two perpendicular crystal axes, d is the flake thickness and λ is the wavelength of the incident light. As such, the slope (i.e., $(2\pi \times \Delta n)/\lambda$) reveals the magnitude of the birefringence. We note that this equation assumes that the material birefringence is independent of the material thickness. This is a reasonable assumption as the thicknesses of our studied flakes are >40 nm.[52] By subtracting δ_0 (i.e., $d = 0$), the phase retardance resulting from BP's birefringence is extracted in Figure S11 (see SI). A maximum retardance of 38° is obtained at 520 nm wavelength with a 220 nm thick BP flake. Given that the monolayer thickness of BP is 0.53 nm,[30] we estimate a phase retardance of ~0.1° (corresponding to ~$\lambda/3600$) per atomic layer (AL). The refractive index difference between the AC and ZZ crystal directions (i.e., Δn, the birefringence) in BP is calculated from the experimental phase retardance results with eq 2 and presented in Figure 3c as a function of the wavelength. We find that Δn is similar (~0.20) at 642 and 730 nm wavelengths, but is larger (~0.24) at 520 nm. This is comparable to the previously reported results on BP[29] (a detailed com

4
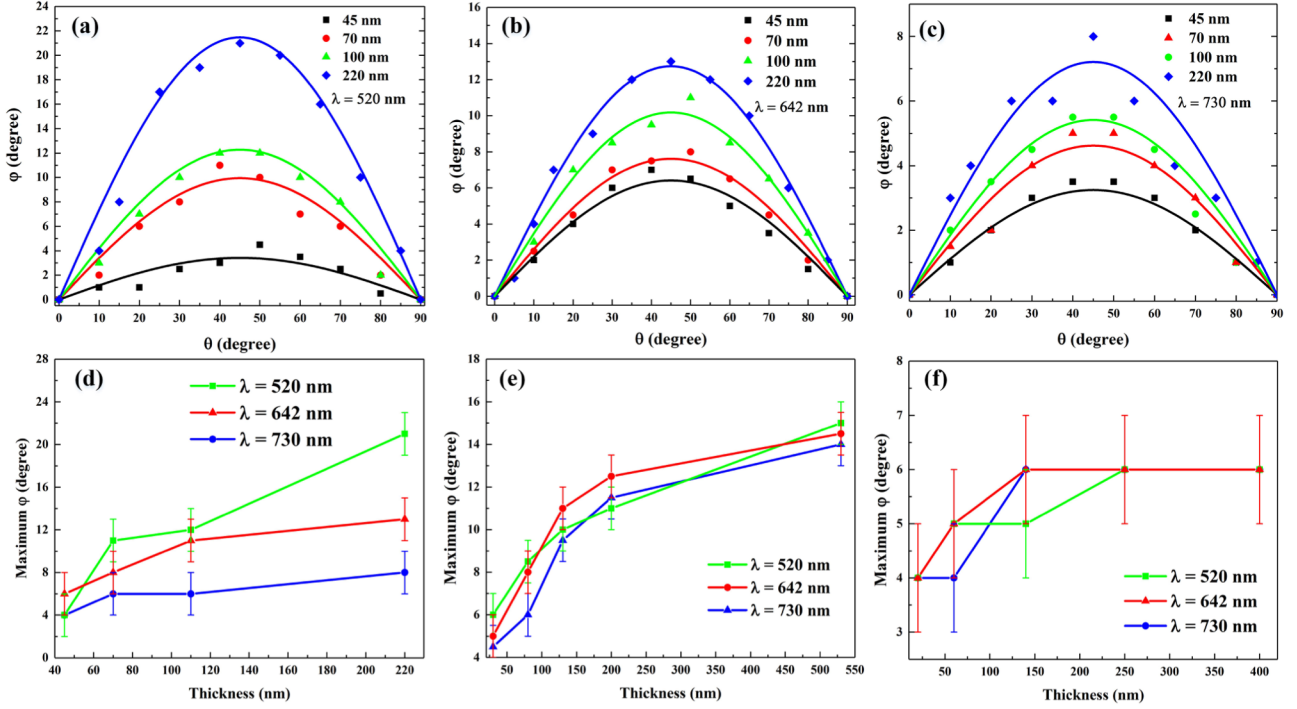
Figure 4 Anisotropic 2D materials based waveplates. Dependence of the polarization-plane rotation angles (φ) for different BP thickness flakes at (a) 520 nm (b) 642 nm and (c) 730 nm separately. The dots are experimental data, while the curves are plotted here to guide the eye. (d), (e) and (f) illustrate the maximum polarization-plane rotation angles (φ) as a function of BP, ReS$_2$ and ReSe$_2$ flake thickness in the visible range, respectively.

parison in Table 1). We also present the theoretically calculated Δn of BP from the dielectric functions within the independent particle approximation on top of the electronic structure that is obtained using hybrid density functions (details in SI).[53] As shown in Figure 3c, the experimentally measured and the theoretically calculated birefringence are in good agreement.

The same birefringence measurement method is also employed for ReS$_2$ and ReSe$_2$. The experimental results and the ellipticity fits are shown in Figures S13 (for ReS$_2$) and S14 (for ReSe$_2$) in SI. The fitted phase retardance as a function of the flake thickness at three wavelengths is presented in Figure 3d (for ReS$_2$) and Figure 3e (for ReSe$_2$). As expected, the two figures illustrate that the phase retardance increases linearly with the flake thickness. By subtracting δ_0 from the incident light with eq 2, we obtain the birefringence induced phase retardance (Figure S13 for ReS$_2$ and S14 for ReSe$_2$ in SI). The results give the maximum retardance of ~0.021°/AL (at the wavelength of 730 nm) for ReS$_2$ and ~0.032°/AL for ReSe$_2$ (at the wavelength of 642 nm), respectively, considering that the atomic layer thickness of both ReS$_2$ and ReSe$_2$ is ~0.7 nm.[54] The birefringence of ReS$_2$ and ReSe$_2$ is then calculated from the experimental phase retardance results with eq 2, and plotted in Figure 3f. This shows that Δn is depended on the wavelength but the difference between ReS$_2$ and ReSe$_2$ is small (<0.03). We propose that this is because the atomic structures and properties of ReS$_2$ and ReSe$_2$ are similar.[55] Note that we are unable to use the density functional theory calculation method (details in SI) used for BP for the case of ReS$_2$ and ReSe$_2$. This is due to their large unit cell and distorted structures. Such theoretical birefringence calculation of ReS$_2$ and ReSe$_2$ requires further study.

For comparison, we list Δn of BP, ReS$_2$, and ReSe$_2$, in Table 1. By comparing Δn of these three anisotropic 2D materials, we find that the birefringence of BP is ~ 6 times larger than that of ReS$_2$ and ReSe$_2$ at 520 nm. This is consistent with our previous PROM results (Figure S3 for BP, Figure S5 for ReS$_2$, Figure S7 for ReSe$_2$), which reveal that the highest contrast (i.e., the largest birefringence) observed among the studied 2D materials in this work comes from BP. Birefringence values of three anisotropic bulk optical materials are also listed in Table 1. This also shows that Δn of BP is comparable to that of the bulk commercial anisotropic materials (e.g., CaCO$_3$). [56]

Waveplates based on anisotropic 2D materials. Birefringence is widely used to make optical waveplates for polarization related applications (e.g., manipulating the polarization state of light[57]). Here, we utilize the birefringence of anisotropic 2D materials for waveplate applications. To measure the rotation of polarization-plane, a key parameter of optical waveplates, we characterize the polarization rotation angle φ of the transmitted light induced by the birefringence (as shown in Figure 2).

Figures 4a-c illustrate the polarization-plane rotation angle of the incident light as a function of the BP flake rotation angle (θ) at three different wavelengths. As illustrated, φ increases with the flake thickness, as the optical path length is longer in the thicker flakes. To clarify the wavelength dependence of φ, the experimentally measured maximum φ values at 520 nm, 642 nm, and 730 nm are presented in Figure 5d. As observed from the flakes with different thicknesses, φ at 520 nm wavelength is larger than that at 642 nm, and is the smallest at 730 nm. The maximum polarization rotation angle at 520 nm wavelength is 21° for the 220

nm thick flake, corresponding to a polarization rotation angle of ~o.o5° /AL. In addition, Δn is wavelength dependent (Figure 3a), indicating chromatic dispersion of BP. This explains the wavelength dependence of φ in Figure 4d. Our results show that the polarization parameters such as phase retardance and polarization-plane rotation can be adjusted with BP flakes, opening its potential for various applications, including optical waveplates as demonstrated here.

The rotation angle of the polarization-plane as a function of the flake thickness of ReS_2 and $ReSe_2$ at three wavelengths is presented in Figures 4e-f, respectively. Similar to what is observed in BP, φ increases with the flake thickness. However, the small difference in φ between ReS_2 and $ReSe_2$ indicates that the birefringence of $ReSe_2$ is slightly larger than that of ReS_2. This agrees well with the previous birefringence measurement (as listed in Table 1). By comparing Figure 4d to Figures 4e-f, φ of ReS_2 and $ReSe_2$ is much smaller than that from BP. This confirms that BP has a larger birefringence than ReS_2 and $ReSe_2$. Therefore, BP offers better polarization control performance over these two anisotropic 2D crystals. We note that there are many other anisotropic 2D layered materials (e.g., GeS,[57] GaTe,[58] SnS,[59] and SnSe[60]), which have been studied to show anisotropic physical responses due to their anisotropic crystal structures. The intrinsic optical birefringence properties of these 2D layered materials also deserve further investigation.

CONCLUSIONS

We demonstrate atomically-thin optical waveplates based on the birefringence of three anisotropic 2D layered materials (BP, ReS_2, and $ReSe_2$). With BP, we observe a polarization-plane rotation of up to ~0.05° per atomic layer at 520 nm. We find that the birefringence of BP is comparable to that of commercially used bulk birefringent materials such as $CaCO_3$ and is ~ 6 times larger than that of ReS_2 and $ReSe_2$. Our results highlight that the relatively large birefringence of anisotropic 2D layered materials such as BP can facilitate accurate manipulation of light polarization with atomically controlled device thickness for various applications where integrated polarization-controllers at the nanoscale are required.

METHODS

Sample preparation and characterization. All flakes (BP, ReS_2, $ReSe_2$) are produced from their bulk crystals by mechanical exfoliation and then transferred onto transparent quartz substrates. The transferred flakes are first characterized by polarized Raman microscopy (WITec Alpha 300 RA) to determine the crystal orientation. Then, a PROM (Leica DM4500) is used to analyse the crystal orientation and capture the optical images under reflection and transmission modes. The custom-built PROM is equipped with fiber coupled visible lasers (Thorlabs, MCLS1) for measurement. A 20X, NA=0.4 objective is used to focus the beam on the flake with ~ 10 μm diameter. During the experiments, all 2D flake samples are characterized immediately after preparation and then kept in the nitrogen box to avoid degradation and/or contamination.

Birefringence measurement process. Three monochromatic continuous wave (CW) lasers at 520 nm, 642 nm, and 730 nm are used as the light sources to test the birefringence of the 2D materials. A polarizer is inserted between the laser source and the flakes to obtain an approximately linearly (with extinction ratio > 30 dB) polarized beam incident on the sample. The exfoliated samples are placed on a rotation stage to change the sample orientation. θ describes the rotation angle between the polarization direction of the incident light and crystal orientation of the flake. After passing through the BP flake, the polarization of the light is examined through a polarization analyser. The schematic diagram of the detection process is illustrated in Figure S8 (see SI). By rotating the analyser, the maximum (I_{max}) and minimum (I_{min}) transmitted light power is recorded with a power detector to examine the ellipticity of the transmitted light. The angle measurement error is ±1°.

AUTHOR INFORMATION

Corresponding Author

* E-mail: zhipei.sun@aalto.fi
ORCID
Zhipei Sun: 0000-0002-9771-5293
Notes
The authors declare no competing financial interest.

REFERENCES

(1) Xia, F.; Wang, H.; Jia, Y., Rediscovering black phosphorus as an anisotropic layered material for optoelectronics and electronics. *Nat. Commun.* **2014**, 5, 4458.
(2) Liu, H.; Neal, A. T.; Zhu, Z.; Luo, Z.; Xu, X.; Tomanek, D.; Ye, P. D., Phosphorene: an unexplored 2D semiconductor with a high hole mobility. *ACS Nano* **2014**, 8, 4033-4041.
(3) Li, L.; Kim, J.; Jin, C.; Ye, G. J.; Qiu, D. Y.; da Jornada, F. H.; Shi, Z.; Chen, L.; Zhang, Z.; Yang, F.; Watanabe, K.; Taniguchi, T.; Ren, W.; Louie, S. G.; Chen, X. H.; Zhang, Y.; Wang, F., Direct observation of the layer-dependent electronic structure in phosphorene. *Nat. Nanotech.* **2017**, 12, 21-25.

(4) Wei, Q.; Peng, X., the Superior mechanical flexibility of phosphorene and few-layer black phosphorus. *Appl. Phys. Lett.* **2014**, 104, 251915.

(5) Wang, X.; Lan, S., Optical properties of black phosphorus. *Adv. Opt. Photonics* **2016**, 8, 618.

(6) Tran, V.; Soklaski, R.; Liang, Y.; Yang, L., Layer-controlled band gap and anisotropic excitons in few-layer black phosphorus. *Phys. Rev. B* **2014**, 89, 235319.

(7) Qiao, J.; Kong, X.; Hu, Z. X.; Yang, F.; Ji, W., High-mobility transport anisotropy and linear dichroism in few-layer black phosphorus. *Nat. Commun.* **2014**, 5, 4475.

(8) Li, D.; Xue, H.; Qi, M.; Wang, Y.; Aksimsek, S.; Chekurov, N.; Kim, W.; Li, C.; Riikonen, J.; Ye, F.; Dai, Q.; Ren, Z.; Bai, J.; Hasan, T.; Lipsanen, H.; Sun, Z., Graphene actively Q-switched lasers. *2D Mater.* **2017**, 4, 025095.

(9) Ferrari, A. C. et.al., Science and technology roadmap for graphene, related two-dimensional crystals, and hybrid systems. *Nanoscale* **2015**, 7, 4598-4810.

(10) Martinez, A.; Sun, Z., Nanotube and graphene saturable absorbers for fibre lasers. *Nat. Commun.,* **2013**, 7, 842-845.

(11) Mak, K. F.; Shan, J., Photonics and optoelectronics of 2D semiconductor transition metal dichalcogenides. *Nat. Photon.* **2016**, 10, 216-226.

(12) Bonaccorso, F.; Sun, Z.; Hasan, T.; Ferrari, A. C., Graphene photonics and optoelectronics. *Nat. Photon.* **2010**, 4, 611-622.

(13) Koppens, F. H.; Mueller, T.; Avouris, P.; Ferrari, A. C.; Vitiello, M. S.; Polini, M., Photodetectors based on graphene, other two-dimensional materials and hybrid systems. *Nat. Nanotech.* **2014**, 9, 780-793.

(14) Wang, Q. H.; Kalantar-Zadeh, K.; Kis, A.; Coleman, J. N.; Strano, M. S., Electronics and optoelectronics of two-dimensional transition metal dichalcogenides. *Nat. Nanotech.* **2012**, 7, 699-712.

(15) Xia, F.; Mueller, T.; Lin, Y. M.; Valdes-Garcia, A.; Avouris, P., Ultrafast graphene photodetector. *Nat. Nanotech.* **2009**, 4, 839-843.

(16) Yang, J.; Wang, Z.; Wang, F.; Xu, R.; Tao, J.; Zhang, S.; Qin, Q.; Luther-Davies, B.; Jagadish, C.; Yu, Z.; Lu, Y., Atomically thin optical lenses and gratings. *Light Sci. Appl.* **2016**, 5, e16046.

(17) Sun, Z.; Martinez, A.; Wang, F., Optical modulators with 2D layered materials. *Nat. Photon.* **2016**, 10, 227-238.

(18) Bonaccorso, F.; Sun, Z., Solution processing of graphene, topological insulators and other 2d crystals for ultrafast photonics. *Opt. Mater. Express* **2014**, 4, 63-78.

(19) A. Saynatjoki; L. Karvonen1; H. Rostami; A. Autere; S. Mehravar; A. Lombardo; R. A.Norwood; T. Hasan; N. Peyghambarian; H. Lipsanen; K. Kieu; A. C. Ferrari; M. Polini; Sun, Z., Ultra-strong nonlinear optical processes and trigonal warping in MoS2 layers. arXiv, 1608.04101.

(20) Karvonen, L.; Saynatjoki, A.; Huttunen, M. J.; Autere, A.; Amirsolaimani, B.; Li, S.; Norwood, R. A.; Peyghambarian, N.; Lipsanen, H.; Eda, G.; Kieu, K.; Sun, Z., Rapid visualization of grain boundaries in monolayer MoS_2 by multiphoton microscopy. *Nat. Commun.* **2017**, 8, 15714.

(21) Luo, Z.; Maassen, J.; Deng, Y.; Du, Y.; Garrelts, R. P.; Lundstrom, M. S.; Ye, P. D.; Xu, X., Anisotropic in-plane thermal conductivity observed in few-layer black phosphorus. *Nat. Commun.* **2015**, 6, 8572.

(22) Aslan, O. B.; Chenet, D. A.; van der Zande, A. M.; Hone, J. C.; Heinz, T. F., Linearly Polarized Excitons in Single- and Few-Layer ReS_2 Crystals. *ACS Photonics* **2016**, 3, 96-101.

(23) Sim, S.; Lee, D.; Noh, M.; Cha, S.; Soh, C. H.; Sung, J. H.; Jo, M. H.; Choi, H., Selectively tunable optical Stark effect of anisotropic excitons in atomically thin ReS_2. *Nat. Commun.* **2016**, 7, 13569.

(24) Zhao, H.; Wu, J.; Zhong, H.; Guo, Q.; Wang, X.; Xia, F.; Yang, L.; Tan, P.; Wang, H., Interlayer interactions in anisotropic atomically thin rhenium diselenide. *Nano Res.* **2015**, 8, 3651-3661.

(25) Cui, Q.; He, J.; Bellus, M. Z.; Mirzokarimov, M.; Hofmann, T.; Chiu, H. Y.; Antonik, M.; He, D.; Wang, Y.; Zhao, H., Transient Absorption Measurements on Anisotropic Monolayer ReS_2. *Small* **2015**, 11, 5565-5571.

(26) Chenet, D. A.; Aslan, O. B.; Huang, P. Y.; Fan, C.; van der Zande, A. M.; Heinz, T. F.; Hone, J. C., In-Plane Anisotropy in Mono- and Few-Layer ReS_2 Probed by Raman Spectroscopy and Scanning Transmission Electron Microscopy. *Nano Lett.* **2015**, 15, 5667-5672.

(27) Lin, Y.-C.; Komsa, H.-P.; Yeh, C.-H.; Bjorkman, T.; Liang, Z.-Y.; Ho, C.-H.; Huang, Y.-S.; Chiu, P.-W.; Krasheninnikov, A. V.; Suenaga, K., Single-Layer ReS_2: Two-Dimensional Semiconductor with Tunable In-Plane Anisotropy. *ACS Nano* **2015**, 9, 11249-11257.

(28) Cui, Q.; Muniz, R. A.; Sipe, J. E.; Zhao, H., Strong and anisotropic third-harmonic generation in monolayer and multilayer ReS_2. *Phys. Rev. B* **2017**, 95, 165406.

(29) Mao, N.; Tang, J.; Xie, L.; Wu, J.; Han, B.; Lin, J.; Deng, S.; Ji, W.; Xu, H.; Liu, K.; Tong, L.; Zhang, J., Optical Anisotropy of Black Phosphorus in the Visible Regime. *J. Am. Chem. Soc.* **2016**, 138, 300-305.

(30) Wang, X.; Jones, A. M.; Seyler, K. L.; Tran, V.; Jia, Y.; Zhao, H.; Wang, H.; Yang, L.; Xu, X.; Xia, F., Highly anisotropic and robust excitons in monolayer black phosphorus. *Nat. Nanotech.* **2015**, 10, 517-521.

(31) Yuan, H.; Liu, X.; Afshinmanesh, F.; Li, W.; Xu, G.; Sun, J.; Lian, B.; Curto, A. G.; Ye, G.; Hikita, Y.; Shen, Z.; Zhang, S. C.; Chen, X.; Brongersma, M.; Hwang, H. Y.; Cui, Y., Polarization-sensitive broadband photodetector using a black phosphorus vertical p-n junction. *Nat. Nanotech.* **2015**, 10, 707-713.

(32) Lan, S.; Rodrigues, S.; Kang, L.; Cai, W., Visualizing Optical Phase Anisotropy in Black Phosphorus. *ACS Photonics* **2016**, 3, 1176-1181.

(33) Ribeiro, H. B.; Pimenta, M. A.; Matos, C. J. S. d.; Moreira, R. L.; Rodin, A. S.; Zapata, J. D.; Souza, E. z. A. T. d.; Neto, A. H. C., Unusual angular dependence of the Raman response in black phosphorus. *ACS Nano* **2015**, 9, 4270-4276.

(34) Kim, J.; Lee, J. U.; Lee, J.; Park, H. J.; Lee, Z.; Lee, C.; Cheong, H., Anomalous polarization dependence of Raman scattering and crystallographic orientation of black phosphorus. *Nanoscale* **2015**, 7, 18708-18715.

(35) Wu, J.; Mao, N.; Xie, L.; Xu, H.; Zhang, J., Identifying the crystalline orientation of black phosphorus using angle-resolved polarized Raman spectroscopy. *Angew. Chem. Int. Ed. Engl.* **2015**, 54, 2366-2369.

(36) Ling, X.; Huang, S.; Hasdeo, E. H.; Liang, L.; Parkin, W. M.; Tatsumi, Y.; Nugraha, A. R.; Puretzky, A. A.; Das, P. M.; Sumpter, B. G.; Geohegan, D. B.; Kong, J.; Saito, R.; Drndic, M.; Meunier, V.; Dresselhaus, M. S., Anisotropic Electron-Photon and Electron-Phonon Interactions in Black Phosphorus. *Nano Lett.* **2016**, 16, 2260-2267.

(37) Mao, N.; Wu, J.; Han, B.; Lin, J.; Tong, L.; Zhang, J., Birefringence-Directed Raman Selection Rules in 2D Black Phosphorus Crystals. *Small* **2016**, 12, 2627-2633.

(38) Zhang, S.; Yang, J.; Xu, R.; Wang, F.; Li, W.; Ghufran, M.; Zhang, Y. W.; Yu, Z.; Zhang, G.; Qin, Q.; Lu, Y., Extraordinary photoluminescence and strong temperature/angle-dependent Raman responses in few-layer phosphorene. *ACS Nano* **2014**, 8, 9590-9596.

(39) Li, D.; Jussila, H.; Karvonen, L.; Ye, G.; Lipsanen, H.; Chen, X.; Sun, Z., Polarization and Thickness Dependent Absorption Properties of Black Phosphorus: New Saturable Absorber for Ultrafast Pulse Generation. *Sci. Rep.* **2015**, 5, 15899.

(40) Mas-Balleste, R.; Gomez-Navarro, C.; Gomez-Herrero, J.; Zamora, F., 2D materials: to graphene and beyond. *Nanoscale* **2011**, 3, 20-30.

(41) Guo, Q.; Pospischil, A.; Bhuiyan, M.; Jiang, H.; Tian, H.; Farmer, D.; Deng, B.; Li, C.; Han, S. J.; Wang, H.; Xia, Q.; Ma, T. P.; Mueller, T.; Xia, F., Black Phosphorus Mid-Infrared Photodetectors with High Gain. *Nano Lett.* **2016**, 16, 4648-55.

(42) Li, D.; Del Rio Castillo, A. E.; Jussila, H.; Ye, G.; Ren, Z.; Bai, J.; Chen, X.; Lipsanen, H.; Sun, Z.; Bonaccorso, F., Black phosphorus polycarbonate polymer composite for pulsed fibre lasers. *Appl. Mater. Today* **2016**, 4, 17-23.

(43) Bonaccorso, F.; Lombardo, A.; Hasan, T.; Sun, Z.; Colombo, L.; Ferrari, A. C., Production and processing of graphene and 2d crystals. *Mater. Today* **2012**, 15, 564-589.

(44) Castellanos-Gomez, A.; Vicarelli, L.; Prada, E.; Island, J. O.; Narasimha-Acharya, K. L.; Blanter, S. I.; Groenendijk, D. J.; Buscema, M.; Steele, G. A.; Alvarez, J. V.; Zandbergen, H. W.; Palacios, J. J.; van der Zant, H. S. J., Isolation and characterization of few-layer black phosphorus. *2D Mater.* **2014**, 1, 025001.

(45) Dresselhaus, M. S.; Dresselhaus, G.; Saito, R.; Jorio, A., Raman spectroscopy of carbon nanotubes. *Phys. Rep.* **2005**, 409, 47-99.

(46) Yang, H.; Fu, B.; Li, D.; Tian, Y.; Chen, Y.; Mattila, M.; Yong, Z.; Li, R.; Hassanien, A.; Yang, C.; Tittonen, I.; Ren, Z.; Bai, J.; Li, Q.; Kauppinen, E. I.; Lipsanen, H.; Sun, Z., Broadband laser polarization control with aligned carbon nanotubes. *Nanoscale* **2015**, 7, 11199-11205.

(47) Lee, K. F.; Tian, Y.; Yang, H.; Mustonen, K.; Martinez, A.; Dai, Q.; Kauppinen, E. I.; Malowicki, J.; Kumar, P.; Sun, Z., Photon-Pair Generation with a 100 nm Thick Carbon Nanotube Film. *Adv. Mater.* **2017**, 1605978.

(48) Y. Akahama, M. K. a. H. K., Raman study of black phosphorus up to 13 GPa. *Solid State Commun.* **1997**, 104, 311-315.

(49) Heyd, J.; Scuseria, G. E.; Ernzerhof, M., Hybrid functionals based on a screened Coulomb potential. *J. Chem. Phys.* **2003**, 118, 8207-8215.

(50) Ares, P.; Zamora, F.; Gomez-Herrero, J., Optical Identification of Few-Layer Antimonene Crystals. *ACS Photonics* **2017**, 4, 600-605.

(51) Chen, H.; Fei, W.; Zhou, J.; Miao, C.; Guo, W., Layer Identification of Colorful Black Phosphorus. *Small* **2017**, 13, 1602336.

(52) Low, T.; Rodin, A. S.; Carvalho, A.; Jiang, Y.; Wang, H.; Xia, F.; Castro Neto, A. H., Tunable optical properties of multilayer black phosphorus thin films. *Phys. Rev. B* **2014**, 90, 075434.

(53) Autere, A.; Ryder, C. R.; Saynatjoki, A.; Karvonen, L.; Amirsolaimani, B.; Norwood, R. A.; Peyghambarian, N.; Kieu, K.; Lipsanen, H.; Hersam, M. C.; Sun, Z., Rapid and Large-Area Characterization of Exfoliated Black Phosphorus Using Third-Harmonic Generation Microscopy. *J. Phys. Chem. Lett.* **2017**, 8, 1343-1350.

(54) Zhong, H.-X.; Gao, S.; Shi, J.-J.; Yang, L., Quasiparticle band gaps, excitonic effects, and anisotropic optical properties of the monolayer distorted 1T diamond-chain structures ReS_2 and $ReSe_2$. *Phys. Rev. B* **2015**, 92, 115438.

(55) Wen, W.; Zhu, Y.; Liu, X.; Hsu, H. P.; Fei, Z.; Chen, Y.; Wang, X.; Zhang, M.; Lin, K. H.; Huang, F. S.; Wang, Y. P.; Huang, Y. S.; Ho, C. H.; Tan, P. H.; Jin, C.; Xie, L., Anisotropic Spectroscopy and Electrical Properties of 2D $ReS_{2(1-x)}Se_{2x}$ Alloys with Distorted 1T Structure. *Small* **2017**, 13, 1603788.

(56) Elert, G., Refraction, The Physics Hypertextbook. **1998**.

(57) https://www.thorlabs.com/newgrouppage9.cfm?objectgroup_id=7234

(58) Tan, D.; Lim, H. E.; Wang, F.; Mohamed, N. B.; Mouri, S.; Zhang, W.; Miyauchi, Y.; Ohfuchi, M.; Matsuda, K., Anisotropic optical and electronic properties of two-dimensional layered germanium sulfide. *Nano Res.* **2016,** *10*, 546-555.

(59) Huang, S.; Tatsumi, Y.; Ling, X.; Guo, H.; Wang, Z.; Watson, G.; Puretzky, A. A.; Geohegan, D. B.; Kong, J.; Li, J.; Yang, T.; Saito, R.; Dresselhaus, M. S., In-Plane Optical Anisotropy of Layered Gallium Telluride. *ACS Nano* **2016,** *10*, 8964-8972.

(60) Tian, Z.; Guo, C.; Zhao, M.; Li, R.; Xue, J., Two-Dimensional SnS: A Phosphorene Analogue with Strong In-Plane Electronic Anisotropy. *ACS Nano* **2017,** *11*, 2219-2226.

(61) Xu, X.; Song, Q.; Wang, H.; Li, P.; Zhang, K.; Wang, Y.; Yuan, K.; Yang, Z.; Ye, Y.; Dai, L., In-Plane Anisotropies of Polarized Raman Response and Electrical Conductivity in Layered Tin Selenide. *ACS Appl. Mater. Interfaces* **2017,** *9*, 12601-12607.
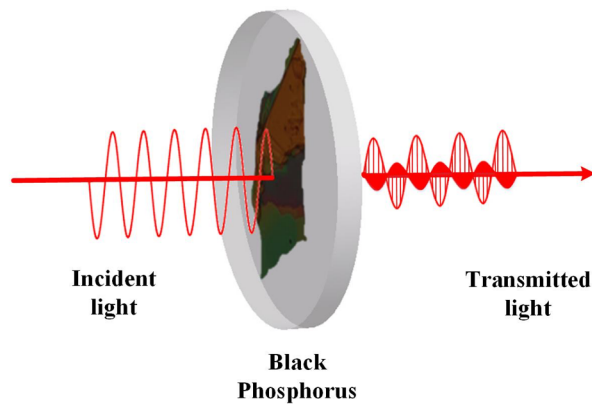
Optical waveplates based on birefringence of anisotropic two-dimensional layered materials

He Yang, Henri Jussila, Anton Autere, Hannu-Pekka Komsa, Guojun Ye, Xianhui Chen, Tawfique Hasan, and Zhipei Sun

Table of Contents (TOC)

The polarization state of the light can be changed after it propagates through a black phosphorus flake due to the intrinsic birefringence property of black phosphorus.